

Are your **MRI contrast agents** cost-effective?

Learn more about generic **Gadolinium-Based Contrast Agents**.



**FRESENIUS
KABI**

caring for life

AJNR

This information is current as
of May 3, 2024.

Feasibility and Added Value of Fetal DTI Tractography in the Evaluation of an Isolated Short Corpus Callosum: Preliminary Results







A.-E. Millischer, D. Grevent, P. Sonigo, N. Bahi-Buisson, I. Desguerre, H. Mahallati, J.-P. Bault, T. Quibel, S. Couderc, M.-L. Moutard, E. Julien, V. Dangouloff, B. Bessieres, V. Malan, T. Attie, L.-J. Salomon and N. Boddaert

AJNR Am J Neuroradiol 2022, 43 (1) 132-138

doi: <https://doi.org/10.3174/ajnr.A7383>

<http://www.ajnr.org/content/43/1/132>

Feasibility and Added Value of Fetal DTI Tractography in the Evaluation of an Isolated Short Corpus Callosum: Preliminary Results

 A.-E. Millischer,  D. Grevent, P. Sonigo, N. Bahi-Buisson,  I. Desguerre,  H. Mahallati, J.-P. Bault, T. Quibel,  S. Couderc, M.-L. Moutard, E. Julien, V. Dangouloff, B. Bessieres, V. Malan, T. Attie, L.-J. Salomon, and  N. Boddaert



ABSTRACT

BACKGROUND AND PURPOSE: Prognosis of isolated short corpus callosum is challenging. Our aim was to assess whether fetal DTI tractography can distinguish callosal dysplasia from variants of normal callosal development in fetuses with an isolated short corpus callosum.

MATERIALS AND METHODS: This was a retrospective study of 37 cases referred for fetal DTI at 30.4 weeks (range, 25–34 weeks) because of an isolated short corpus callosum less than the 5th percentile by sonography at 26 weeks (range, 22–31 weeks). Tractography quality, the presence of Probst bundles, dysmorphic frontal horns, callosal length (internal cranial occipitofrontal dimension/length of the corpus callosum ratio), and callosal thickness were assessed. Cytogenetic data and neurodevelopmental follow-up were systematically reviewed.

RESULTS: Thirty-three of 37 fetal DTIs distinguished the 2 groups: those with Probst bundles (Probst bundles+) in 13/33 cases (40%) and without Probst bundles (Probst bundles-) in 20/33 cases (60%). Internal cranial occipitofrontal dimension/length of the corpus callosum was significantly higher in Probst bundles+ than in Probst bundles-, with a threshold value determined at 3.75 for a sensitivity of 92% (95% CI, 77%–100%) and specificity of 85% (95% CI, 63%–100%). Callosal lipomas (4/4) were all in the Probst bundles- group. More genetic anomalies were found in the Probst bundles+ than in Probst bundles- group (23% versus 10%, $P = .08$).

CONCLUSIONS: Fetal DTI, combined with anatomic, cytogenetic, and clinical characteristics could suggest the possibility of classifying an isolated short corpus callosum as callosal dysplasia and a variant of normal callosal development.

ABBREVIATIONS: CC = corpus callosum; FA = fractional anisotropy; fDTI = fetal DTI; fMRI = fetal MR imaging; ICOFD/LCC = internal cranial occipitofrontal dimension/length of the corpus callosum; ISCC = isolated short corpus callosum; IQR = interquartile range; PB = Probst bundles; SCC = short corpus callosum

The corpus callosum (CC) is the midline commissural white matter tract that connects the 2 cerebral hemispheres. It


continues to grow throughout pregnancy and even throughout infancy.¹ At the end of the first trimester, it takes on its usual curvilinear shape.² Improvements in fetal sonography have led to a wide range of diagnoses of callosal abnormalities, from complete callosal agenesis to partial agenesis, thick and thin corpus callosums, and hypoplasia of the corpus callosum, recently summarized as callosal dysplasia.³ The characterization of these anomalies relies primarily on biometric criteria of length or thickness.

Short CC (SCC) represents the most frequent anomaly. Although all parts of the CC should be present by 22 weeks' gestational age, exuberant axonal growth continues until 2 months after birth⁴ and final remodeling is achieved by 3 years of age.⁵ Changes in developmental maturity are readily noted in the corpus callosum, and interindividual variations can be observed, particularly involving the body and isthmus.^{6,7} In such cases, the prenatal anatomic integrity of these short corpus callosums cannot be assured, and prenatal counseling is, therefore, challenging.

Received July 14, 2021; accepted after revision September 27.

From the Department of Paediatric Radiology (A.-E.M., D.G., P.S., V.D., N.B.), Assistance Publique-Hôpitaux de Paris, Hôpital Necker Enfants Malades, Université de Paris, Paris France; Institut Imagine (A.-E.M., D.G., P.S., N.B.-B., I.D., V.D., N.B.), Institut National de la Santé et de la Recherche Médicale U1163, Université de Paris, Paris, France; LUMIERE Platform (A.-E.M., D.G., P.S., H.M., N.B., L.-J.S.), Paris, France; IMPC Bachaumont (A.-E.M.), Paris, France; Departments of Pediatric Neurology (N.B.-B., I.D.), Anatomical Pathology (B.B.), and Genetics (V.M., T.A.), Necker Enfants Malades University Hospital, Université de Paris, Paris, France; Departments of Gynecology and Obstetrics (J.-P.B., T.Q.) and Pediatrics (S.C.), CHI, Poissy Saint-Germain, France; Department of Pediatric Neurology (M.-L.M.), Trousseau Hospital, CHU, Trousseau, Paris; Department of Gynecology-Obstetrics (E.J.), Hospital Le Mans, Le Mans, France; Department of Gynecology-Obstetrics (L.-J.S.), Université de Paris, Paris, France; and Department of Radiology (H.M.), University of Calgary, Calgary, Alberta, Canada.

Please address correspondence to Anne-Elodie Millischer, MD, Radiology Department, Hopital Necker enfant Malades, 149 rue de Sèvres 75015 Paris, France; e-mail: aemillischer@gmail.com

 Indicates article with online supplemental data.

<http://dx.doi.org/10.3174/ajnr.A7383>

The prognosis in patients with callosal dysplasia is not clear. It may be associated with varying degrees of neurodevelopmental delay, which are more severe if additional brain anomalies are present. Neurodevelopmental outcome of a short CC in the fetus is uncertain, and its significance is not well-established.^{8,9}

Postnatal MR imaging is widely used to characterize corpus callosal dysplasia. Among the MR imaging sequences used, DTI enables the reconstruction of normal and abnormal fiber bundles (fiber-tracking or tractography). Its application in complete or partial CC agenesis and CC hypoplasia, and a thin CC has shown the consistent presence of Probst bundles (PB).¹⁰ These abnormal bundles, oriented anterior-posteriorly, are thought to result from the lack of transverse decussation within a dysplastic corpus callosum.^{11,12}

Similar to findings in postnatal imaging, PB may also be identified using DTI tractography in the prenatal period.^{13,14} This additional presence of PB can be used to differentiate CC dysplasia from other forms of isolated short corpus callosum (ISCC) without PB and normal findings on genetic testing, which might reflect variants of normal callosal development. To avoid the dilemma of which callosal biometric curves to rely on, we used the internal cranial occipitofrontal dimension/length of the corpus callosum (ICOFD/LCC) ratio to define a SCC compared with the normal index (2.35 [SD, 0.11]).¹⁵

Therefore, the purpose of this study was 2-fold: first, though it has already been illustrated in 16 cases previously by Kasprian et al,¹⁶ to routinely assess the feasibility of visualizing the presence or absence of PB in fetal MR imaging (fMRI) DTI tractography on a larger cohort, and second, to assess its added value in differentiating CC dysplasia from variants of normal callosal development.

MATERIALS AND METHODS

Study Design

This study was a retrospective review in 2 tertiary level fetal medicine referral centers (Necker Hospital and Poissy Hospital, Paris, France) in a 4-year period from November 2016 to January 2020. We retrospectively analyzed all fMRI studies of fetuses referred for an SCC. The inclusion criteria were fetal imaging of a single pregnancy with a CC length below the 5th percentile according to the reference charts of Achiron and Achiron² for which the integrity of the morphology could not be guaranteed by the referring fetal imaging radiologists in our center. The exclusion criteria were complete agenesis of the CC, an SCC associated with other brain anomalies on MR imaging, or incomplete data.

Data were obtained from the medical records and included maternal history and prenatal history (sex, genetic testing, *Toxoplasma gondii*, other agents, rubella, cytomegalovirus [TORCH serology; Bio-Rad]). Postnatal outcomes included pathologic records when termination of pregnancy was performed, follow-up of neurologic development by the Denver Developmental Screening Test,¹⁷ and postnatal MR imaging including tractography.

fMRI Examinations

MR imaging was performed on 1.5T MR imaging units (Optima MR 450w 1.5T, GE Healthcare, or Aera 1.5T, Siemens) using a phased-array body coil. The patients were placed in a supine or

lateral decubitus position. No maternal sedative or contrast agents were used.

Neuroanatomic Imaging

MR imaging protocol included 3 planes adjusted in real time and customized to the head of each fetus (coronal, sagittal, and axial) with a balanced half Fourier–acquisition single-shot turbo spin-echo HASTE sequence (TR/TE, 4000/86; matrix, 256 × 256; flip angle, 125°; signal average, 1; section thickness, 3 mm; section gap, 30%).

Anatomic Measurements

CC length was systematically evaluated using the ICOFD/LCC ratio compared with the normal index (2.35 [SD, 0.11]).¹⁵ The length of the CC was measured in the midsagittal plane from the most anterior aspect of the genu to the most posterior aspect of the splenium. The ICOFD was measured on the same plane; the calipers were placed on the internal calvarial borders, along the same line that was used to measure the length of the CC.

For dysmorphic features, the presence or absence of an eversion of the frontal horns (Steer horn or Viking Helmet appearance) and colpocephaly was reported systematically.

Callosal thickness was systematically measured in the mid-coronal plane. The corpus callosum was regarded as thick if its midpart measured >2 SDs and thin if it was <2 SDs.²

For the fetal DTI (fDTI) protocol, axial slices were positioned orthogonal to the fetal brainstem. The basic settings of the DTI sequence were identical for the 2 MR imaging devices used. For DTI acquisitions, an axial, single-shot, echo-planar imaging sequence was used (TR = 2200 ms, TE = 63 ms, acquisition matrix = 112 × 112 re-sampled to 256 × 256, voxel size = 1 × 1 mm, section thickness = 3–5 mm without a gap or interleaved slices). For each of the DTI scans, 15 noncolinear direction diffusion-weighted magnetic-pulsed gradients were used with a b-value = 700 s/mm², and 1 B₀ image without diffusion-weighting was also obtained. Fifteen slices were recorded during an overall imaging time of 2 minutes of scanning.

Fetal-Specific Postprocessing of DTI Data

For tractography, we used a deterministic linear tracking algorithm with the following cutoff values: minimum fractional anisotropy (FA) (FA threshold) = 0.10–0.15; maximum angle change (angle threshold) = 27.0°–45.0°; and minimum fiber length = 10 mm. No advanced motion correction was used.¹⁸ Tractography was first attempted with minimum thresholds of FA = 0.15 and angle = 27°. If tractography was not satisfactory with those standard parameters, the FA threshold was lowered to 0.10 and/or the angle threshold was increased to 45°.¹⁹

Only 1 senior radiologist performed the fDTI analysis (A.-E.M.), a radiologist with 15 years of experience in the field of fetal MR imaging (about 380 scans/year) and neuropediatrics. To trace the fibers crossing at the CC, a polygonal ROI was drawn in the midsagittal plane of each subject, encompassing the entire CC. For the PB, the fiber trajectory was not known a priori, except in its middle portion, where it clearly showed a rostrocaudal direction in the anatomic images and in the color-coded FA maps, creating the roof of the lateral ventricles.²⁰ To determine

the potential connectivity of the callosal remnant in each patient with an SCC, we drew single irregular polygonal ROIs encompassing the entire remnant area in the axial plane, focused on the regions of the centra semiovale. The ROIs were drawn manually according to anatomic landmarks. The examination was considered to be uninterpretable and de facto excluded by the radiologist when fetal motion artifacts interfered with interpretation of fDTIs.

Postnatal MR imaging, when applicable, was systematically performed by an experienced radiologist blinded to the prenatal data between 0 and 12 months, to confirm the prenatal fMRI data and to exclude any other brain anomalies. Three planes of FSE T2-weighted, 3D echo-spoiled gradient echo T1-weighted, and DTI tractography scans were performed on the Optima 1.5T MR imaging unit. For each of the DTI scans, 40 noncollinear-direction diffusion-weighted magnetic-pulsed gradients were used with a b-value of 700 s/mm².

Genetics Analyses

All fetuses were studied by karyotyping and chromosomal microarray analysis with DNA extracted from amniotic fluid. Informed consent for genetic studies was obtained from all pregnant women. Different types of microarrays were used by the centers: Agilent 60k (Agilent Technologies) and Agilent 180k and CytoScan 750K (SNP arrays, Affymetrix). Fluorescence in situ hybridization analysis or quantitative polymerase chain reaction were performed on the fetus to confirm the detected copy number variations and on the parents to determine the fetus's inheritance. The American College of Medical Genetics and Genomics/Clinical Genome guidelines were used to assess copy number variations pathogenicity.²¹

Outcomes

Terminations of pregnancy were all performed in accordance with French laws, and pathologic assessment and postmortem examinations were systematically performed.

In cases of live birth, the neurodevelopmental outcome was evaluated by a specialist in pediatric neurology (N.B.-B.), who evaluated communication skills, daily living skills, socialization skills, and motor skills based on the international Denver Developmental Screening Test.^{8,22}

Scores were considered abnormal if the standard score was <85. The mean age at follow-up was 21.5 months for PB+ and 15.2 months for PB-.

Statistical Analysis

Statistical analyses were conducted using ad hoc routines implemented in R 4.0.0 software (<http://www.r-project.org>). Data description was performed using median and interquartile range (IQR) for quantitative data (ICOFD/LCC ratio and thickness of the CC). Median values were compared between patients with the presence of PB (PB+) and no PB (PB-), using the nonparametric Wilcoxon rank-sum test. The pROC package (<https://rdrr.io/cran/pROC/man/pROC-package.html>) for receiver operating characteristic curve analysis and calculation of sensitivities and specificities assessed the diagnostic performance. A bootstrap method was used to calculate the 95% CI of the area under the receiver operating characteristic curves, sensitivities, and specificities. All tests were 2-sided, with α set at 5%.

Ethics Approval

The local (DPO-APHP, France) institutional ethics board approved the study: institutional review board registration 00011928 (CERAPH 2020-12-06).

RESULTS

The study population included 37 fMRIs with fDTI tractography performed for ISCC at a median gestational age of 30.4 weeks (range, 25-34 weeks). There were 23 male (62%) and 14 female (37%) fetuses. DTI was feasible in all but 4/37 fetuses (11%) (Online Supplemental Data).

Pathology

Eleven of 33 terminations of pregnancy were performed. These included 9 cases of PB+, which represented 69% (9/13) of all cases of PB+ in our series, and 2 cases of PB-, which represented 10% (2/20) of all cases of PB-. No additional brain anomalies were found in any of the cases at postmortem examination.

We followed 22 of 33 neonates: One of 22 had a borderline psychomotor development, 1/22 had a delayed psychomotor development, 1/22 was lost to follow-up, and 19/22 had normal psychomotor development.

DTI Tractography and PB

Among the 33 interpretable fDTI tractography studies, PB+ was seen in 13 cases (13/33) versus PB- in 20 cases, demonstrating 2 patterns in our series of ISCC (Fig 1).

When PB were absent (PB-) at fDTI (20/33), this absence of PB was confirmed for all cases on postnatal DTI in 12/12 live births and by postmortem examination in 2/2 cases of termination of pregnancy. The remaining 6/20 patients did not undergo postnatal MR imaging because the pediatric neurologist and/or parents did not think it was warranted in the setting of normal neurologic development.

Among the 13 patients with PB at fDTI (PB+), the presence of PB was confirmed in all cases on postnatal DTI in 3/3 live births and by postmortem examination in 9/9 cases of termination of pregnancy. One of 13 patients was lost to follow-up. Discrimination between the cingulum and the PB was appreciated on color-coded maps: The cingulum presented in a well-recognized inferior-superior direction, and PBs presented in a typical anterior-posterior direction, as mentioned in the literature.¹⁶

Neuroanatomic Description between PB+ and PB- Populations

The ICOFD/LCC ratio was significantly greater in cases of PB+, 4.7 (IQR, 4.3-6.0) versus 3.4 in cases of PB- (IQR, 3.3-3.7; $P < .001$, $P = .0007$). A threshold value of 3.75 could help distinguish between cases with or without PB with a sensitivity of 92% (95% CI, 77%-100%) and a specificity of 85% (95% CI, 63%-100%) (Fig 2).

A biconvex dysmorphic appearance (Steer horn or Viking helmet) of the frontal ventricular horns was noted in 100% (13/13) of cases of PB+ and was absent in 95% (19/20) of cases of PB- ($P < .001$).

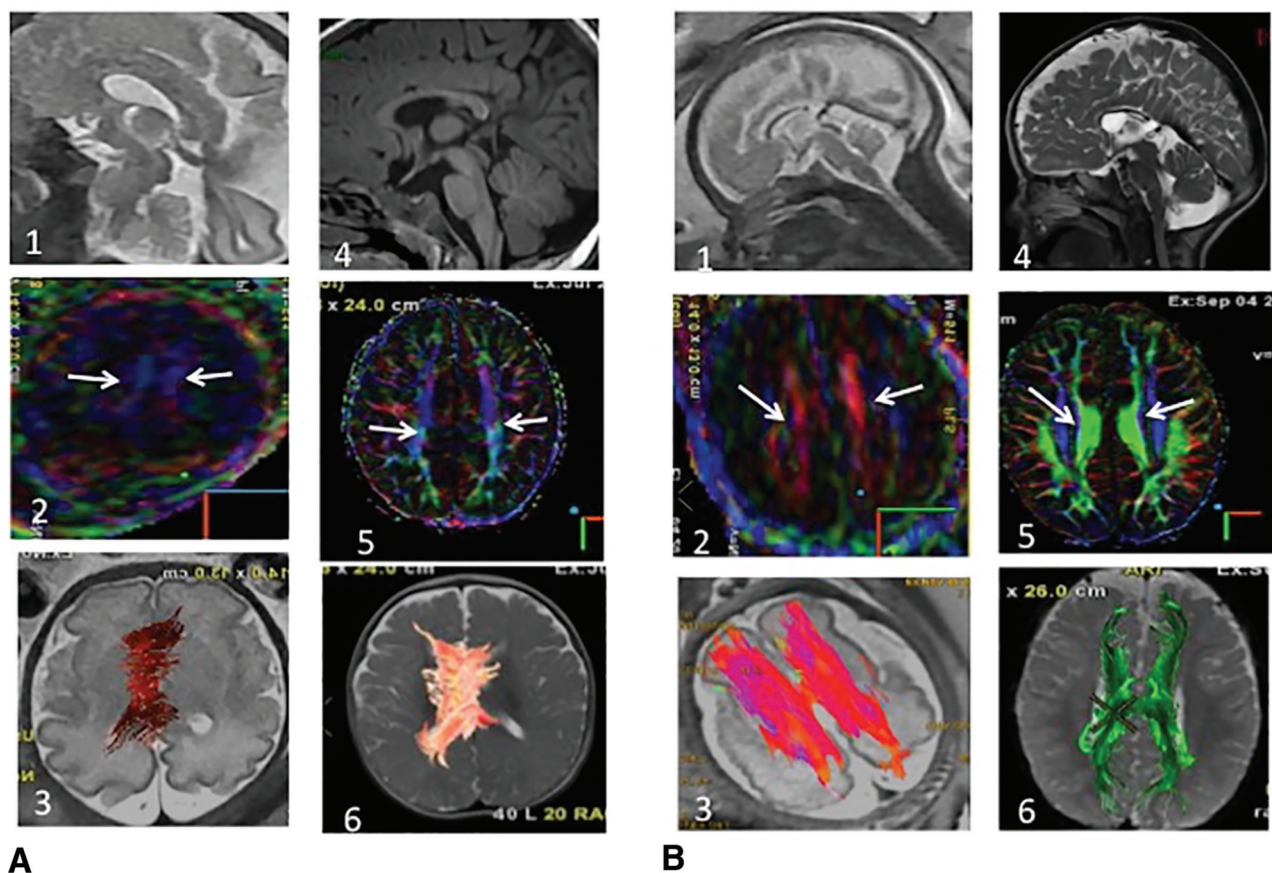


FIG 1. Fetal (30 weeks) and postnatal anatomic MR imaging and DTI (6 months) of ISCC PB⁻ (A) and PB⁺. *A1*, Sagittal single-shot fast spin-echo T2 (SSFSET2) shows an ISCC. *A2*, DTI color-coding map shows the absence of PB, confirmed in postnatal imaging (*A3–6*). Only the cingulum is present, well-recognized by the inferior-superior direction in blue (*white arrows*), present on pre- and postnatal imaging. *B1*, Sagittal SSFSET2 shows an ISCC. *B2*, DTI color-coding map shows the presence of PB (*white arrows*), confirmed by a postnatal color-coding map (*B3–6*). PB are identified by their typical anterior-posterior orientation on the color-coding maps (*B2* and *B5*). Fiber-tracking demonstrates the typical anterior-posterior thick PB, with a remnant of the left-to-right CC (*B3* and *B6*).

Abnormal thickness of the corpus callosum was found in 23% ($n = 3/13$) of PB⁺ and 25% ($n = 5/20$) of PB⁻. No significant difference was found in the distribution of thick or thin corpus callosums related to the presence of PB, among the 2 populations (median, 1.7; IQR, 1–3, versus median, 2.2; IQR, 2–3.2; $P < .10$).

Among the 8 thick corpus callosums, postnatal MR imaging diagnosed 4 callosal lipomas, all among the 5 thick CCs in the PB⁻ group (4/5). No lipomas were identified among the 3 cases of thick corpus callosum in the PB⁺ population.

Neurologic Evaluation

Among the 4 PB⁺ live births, the median age was 21.5 months (IQR, 15–36 months), 2/4 had a normal psychomotor development at 2.5 years and 15 months of age, respectively. One of 4 had a borderline developmental delay at 3 years, and 1 of 4 was lost to follow-up.

Among the 18 cases of PB⁻, the median age was 15.3 months (IQR, 3–36 months), 17/18 had a normal psychomotor development (94%), and 1 had a delayed psychomotor development thought to be secondary to trisomy 21.

No significant differences were observed between these 2 populations within the limits of the neurologic evaluation period ($P = .27$; OR, 0.14; 95% CI, 0.0014–13.82).

Genetic Anomalies

There were 5 genetic anomalies: 23% (3/13) in the PB⁺ group and 10% (2/20) in the PB⁻ group ($P = .08$). In the PB⁺ group, we found the following: 1) A 8q21.12q21.3 duplication, 11.4 Mb, was detected in the fetus. The genomic position of this copy number variant was $\text{arr}[\text{GRCh37}] \ 8\text{q}21.12\text{q}21.3 \ (79321132_90690216) \times 3 \ \text{dn}$. This anomaly occurred de novo. 2) A fetus was found to have a pericentric inversion of chromosome 18, which arose de novo. The karyotype of the fetus was $46, \text{XX}, \text{inv}(18)(\text{p}11.31\text{q}21.2)$. 3) A de novo 14q12q21.2 deletion was detected in another fetus. The deletion was 16 Mb: $\text{arr}[\text{GRCh37}] \ 14\text{q}12\text{q}21.2(30273044_46669990) \times 1 \ \text{dn}$, a mutation of Zinc finger E-box-binding homeobox 1, a case of deletion 14q12q21. 4) A case of duplication 3q21 Zinc finger E-box-binding homeobox 1 mutation was found in one fetus. 5) A case of duplication 8q211q21.3 was found in one fetus.

In the PB⁻ group, 1 case of trisomy 21 and 1 case of mutation 18p11.31 to 18q21 were found.

DISCUSSION

To our knowledge, this is the first study that routinely reports the feasibility (about 90%) of visualizing the presence or absence of PB in fDTI tractography in a large cohort. This study demonstrates

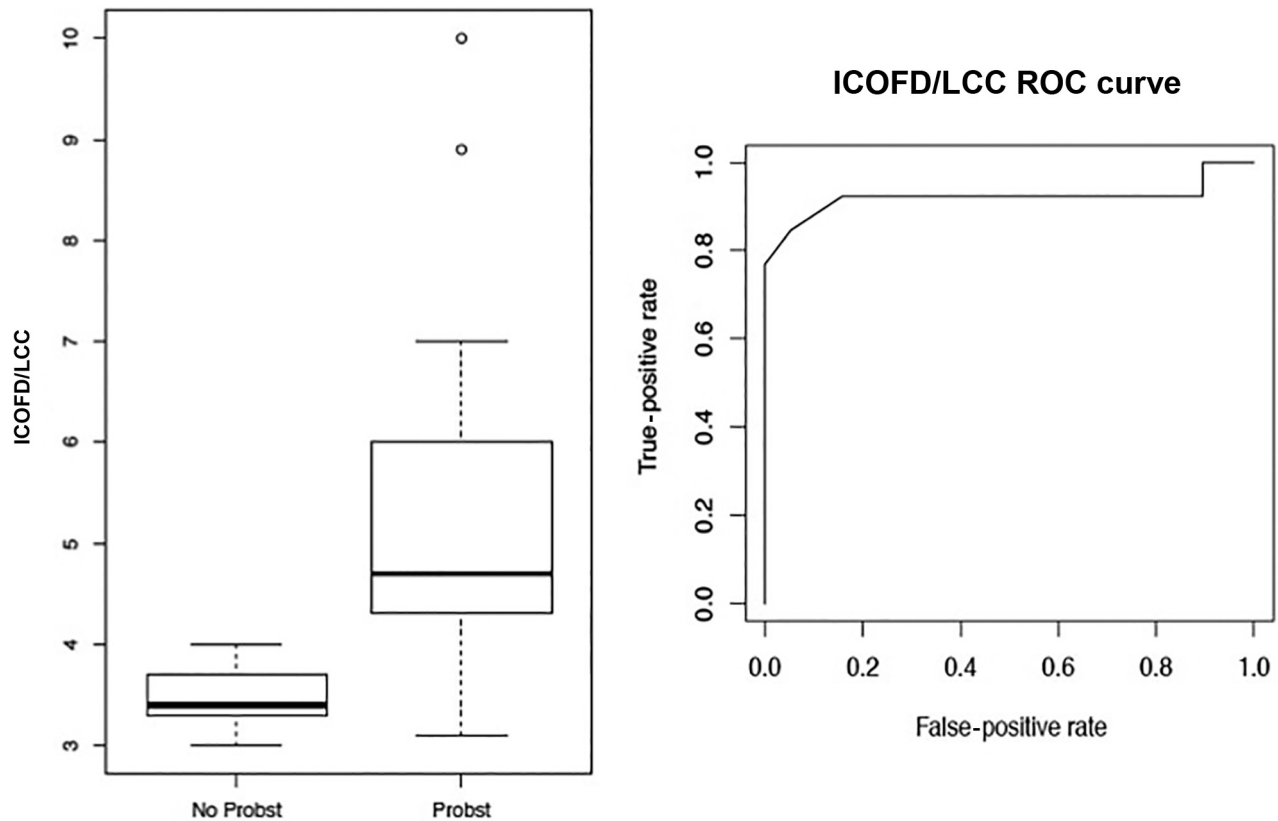


FIG 2. Length of the CC. Dimensions of the CC compared between PB+ and PB-. Boxplot and receiver operating characteristic curve (ROC) about the ICOFD/LCC ratio.

the added value in differentiating CC dysplasia from variants of normal callosal development with an objective technical tool.

Moreover, our data suggest that 3 important features are associated with the presence or absence of PB:

1) When PB are present, the ICOFD/LCC ratio recently published¹⁵ is usually higher. Accordingly, a value of ≥ 3.75 was associated with the presence of PB+ in $>90\%$ of our cases. This simple and straightforward threshold could be used as a routine first-line tool to characterize fetuses with an ISCC at risk for callosal dysplasia. It is not unexpected that we noted that biconvex dysmorphic frontal ventricular horns were also present in 100% of the PB+ group. These data corroborate the anatomic knowledge regarding lateral ventricles in complete or partial agenesis of the corpus callosum, which is usually displaced from the midline by paired PB that fail to cross the hemispheres and run parallel to the midline as T2 hypointense bundles resulting in the Steer horn or Viking helmet appearance of the ventricles.²³ In our study, on re-review of all of cases of PB+, the appearance of T2-hypointense bands along the inner edge of the frontal ventricular horns was always present. These 3 signs (ICOFD/LCC ratio, dysmorphic frontal ventricular horns, and T2-hypointense bands) could, therefore, be easily used on anatomic images to suggest the presence of PB. Thus, our data show that the presence of the bull horn configuration of the lateral ventricles associated with relative shortening of the corpus callosum is associated with a high probability of finding Probst fascicles using DTI. This advanced technique, therefore, provides an objective criterion for an optimal description of the SCC.

2) Genetic anomalies are more frequent in an ISCC with PB+ (23% versus 10%). This finding correlates well with previously published data suggesting that callosal dysplasias are more often associated with genetic syndromes.^{24,25} However, our results are also in line with the recent literature, which points out that the presence of PB is not necessarily associated with a poor prognosis.²⁶ Accordingly, neurologic follow-up was normal for most children with an ISCC and PB-, suggesting, in our preliminary study, that ISCCs with no PB are more likely to be variants of normal development of the corpus callosum. Regarding the case of trisomy 21 in PB-, the diagnosis was suspected as of the first trimester due to an increased nuchal translucency, for which the couple chose not to pursue any confirmatory prenatal cytogenetic investigations. At least on the basis of the data in our study, we believe this case confirms once again that prenatal genetic exploration is essential for the appropriate classification of ISCC.

3) In the absence of the PB, a thick corpus callosum is usually related to lipomas (4/5 in PB- versus 0/3 in PB+). An antenatal diagnosis of lipoma is often challenging and underdiagnosed because the lipomatous components are difficult to demonstrate on fMRIs and antenatal ultrasound,²⁷⁻²⁹ whereas this entity is well-recognized in the postnatal period on MRI, showing typical hyperintensity on T1-weighted MR images (Online Supplemental Data). Indeed, Chougar et al²⁹ and Atallah et al²⁷ concluded in their fMRI series that the type and size of a lipoma influence prenatal T1 signal intensity, and the variability of the T1 intensity may also be related to fat maturation within the lipoma and

perhaps reflects changes related to gestational age. The corollary of our result in fDTI could be that in a thick corpus callosum without PB on tractography, one might suggest the possibility an “occult” callosal lipoma on fetal imaging. To our knowledge, this is the first antenatal study that highlights this feature in the diagnosis of callosal lipoma. This information can be helpful in prenatal counseling, given the excellent prognosis of callosal lipomas.

On the basis of these results, we believe a new decision tree can be proposed, taking into account the results of MR tractography and genetic studies (Online Supplementary Data). To simplify and standardize the prenatal morphologic classification system, as we proposed in our recent study³ and according to the definitions proposed by Edwards et al,⁴ we would suggest defining an ISCC with a Probst bundle as “callosal dysplasia,” and “variant of normal callosal development” in cases of ISCCs without a Probst bundle and no cytogenetic anomalies. Therefore, the generally favorable prognosis of ISCC, reported by Meidan et al,⁸ can be partly explained by the hypothesis that some of the conditions of fetuses and children followed in their study were true variants of normal and not callosal malformations, in other words, children with a fetal diagnosis of ISCC but without PB. However, the major prognostic element remains the association of abnormalities in the CC, Probst band or not.³⁰

We must acknowledge several limitations in our study. First is the retrospective nature of our study, and the number of cases remains limited, even if this is the first study using fDTI in the investigation of ISCC. Second, the relatively high success rate may be related to the comparatively late gestational age of about 30 weeks. Moreover, it was not possible to obtain a full neurologic follow-up until 6 years of age, with a systematic postnatal MR imaging in all cases.

CONCLUSIONS

The challenge of prenatal differentiation of an ISCC as a variant of normal callosal development from callosal dysplasia can be optimized by the use of DTI tractography in fetal MR imaging. We believe that our results can encourage the systematic use of optimized fDTI tractography for the investigation of ISCCs, to assess the presence or absence of PB. Thus, in addition to the classic MR imaging with morphologic analysis, a new approach and paradigm can be proposed, considering the presence or absence of PB, while prospective studies with long-term and reproducible neurologic follow-up are necessary.

Disclosure forms provided by the authors are available with the full text and PDF of this article at www.ajnr.org.

REFERENCES

1. Nunez S, Mantilla MT, Bermudez S. **Midline congenital malformations of the brain and skull.** *Neuroimaging Clin N Am* 2011;21:429–82, vii [CrossRef Medline](#)
2. Achiron R, Achiron A. **Development of the human fetal corpus callosum: a high-resolution, cross-sectional sonographic study.** *Ultrasound Obstet Gynecol* 2001;18:343–47 [CrossRef Medline](#)
3. Mahallati H, Sotiriadis A, Celestin C, et al. **Heterogeneity in defining fetal callosal pathology: a systematic review.** *Ultrasound Obstet Gynecol* 2021;58:11–18 [CrossRef](#)
4. Edwards TJ, Sherr EH, Barkovich AJ, et al. **Clinical, genetic and imaging findings identify new causes for corpus callosum development syndromes.** *Brain* 2014;137:1579–613 [CrossRef Medline](#)
5. Garel C, Cont I, Alberti C, et al. **Biometry of the corpus callosum in children: MR imaging reference data.** *AJNR Am J Neuroradiol* 2011;32:1436–43 [CrossRef Medline](#)
6. Filippi CG, Cauley KA. **Lesions of the corpus callosum and other commissural fibers: diffusion tensor studies.** *Semin Ultrasound CT MR* 2014;35:445–58 [CrossRef Medline](#)
7. Achiron R, Lipitz S, Achiron A. **Sex-related differences in the development of the human fetal corpus callosum: in utero ultrasonographic study.** *Prenat Diagn* 2001;21:116–20 [Medline](#)
8. Meidan R, Bar-Yosef O, Ashkenazi I, et al. **Neurodevelopmental outcome following prenatal diagnosis of a short corpus callosum.** *Prenat Diagn* 2019;39:477–83 [CrossRef Medline](#)
9. Volpe P, Paladini D, Resta M, et al. **Characteristics, associations and outcome of partial agenesis of the corpus callosum in the fetus.** *Ultrasound Obstet Gynecol* 2006;27:509–16 [CrossRef Medline](#)
10. Le Bihan D. **Intravoxel incoherent motion perfusion MR imaging: a wake-up call.** *Radiology* 2008;249:748–52 [CrossRef Medline](#)
11. Tovar-Moll F, Moll J, de Oliveira-Souza R, et al. **Neuroplasticity in human callosal dysgenesis: a diffusion tensor imaging study.** *Cereb Cortex* 2007;17:531–41 [CrossRef Medline](#)
12. Benezit A, Hertz-Pannier L, Dehaene-Lambertz G, et al. **Organising white matter in a brain without corpus callosum fibres.** *Cortex* 2015;63:155–71 [CrossRef Medline](#)
13. Song JW, Gruber GM, Patsch JM, et al. **How accurate are prenatal tractography results? A postnatal in vivo follow-up study using diffusion tensor imaging.** *Pediatr Radiol* 2018;48:486–98 [CrossRef Medline](#)
14. Jakab A, Tuura R, Kellenberger C, et al. **In utero diffusion tensor imaging of the fetal brain: a reproducibility study.** *Neuroimage Clin* 2017;15:601–12 [CrossRef Medline](#)
15. Tepper R, Leibovitz Z, Garel C, et al. **A new method for evaluating short fetal corpus callosum.** *Prenat Diagn* 2019;39:1283–90 [CrossRef](#)
16. Kasprian G, Brugger PC, Schöpf V, et al. **Assessing prenatal white matter connectivity in commissural agenesis.** *Brain* 2013;136:168–79 [CrossRef Medline](#)
17. Abessa TG, Worku BN, Kibebew MW, et al. **Adaptation and standardization of a Western tool for assessing child development in non-Western low-income context.** *BMC Public Health* 2016;16:652 [CrossRef Medline](#)
18. Machado-Rivas F, Afacan O, Khan S, et al. **Tractography of the cerebellar peduncles in second- and third-trimester fetuses.** *AJNR Am J Neuroradiol* 2021;42:194–200 [CrossRef Medline](#)
19. Mitter C, Prayer D, Brugger PC, et al. **In vivo tractography of fetal association fibers.** *PLoS One* 2015;10:e0119536 [CrossRef Medline](#)
20. Mitter C, Jakab A, Brugger PC, et al. **Validation of in utero tractography of human fetal commissural and internal capsule fibers with histological structure tensor analysis.** *Front Neuroanat* 2015;9:164 [CrossRef Medline](#)
21. Riggs ER, Andersen EF, Cherry AM, et al. **Technical standards for the interpretation and reporting of constitutional copy-number variants: a joint consensus recommendation of the American College of Medical Genetics and Genomics (ACMG) and the Clinical Genome Resource (ClinGen).** *Genet Med* 2020;22:245–57 [CrossRef Medline](#)
22. Elliman AM, Bryan EM, Elliman AD, et al. **Denver developmental screening test and preterm infants.** *Arch Dis Child* 1985;60:20–24 [CrossRef Medline](#)
23. Leombroni M, Khalil A, Liberati M, et al. **Fetal midline anomalies: diagnosis and counselling, Part 1: corpus callosum anomalies.** *Eur J Paediatr Neurol* 2018;22:951–62 [CrossRef Medline](#)
24. Das S, Bhansali A, Dutta P, et al. **An unusual association of corpus callosum agenesis in a patient with acromegaly.** *BMJ Case Rep* 2010;2010:bcr012010265 [CrossRef Medline](#)

25. Paul LK, Brown WS, Adolphs R, et al. **Agenesis of the corpus callosum: genetic, developmental and functional aspects of connectivity.** *Nat Rev Neurosci* 2007;8:287–99 [CrossRef Medline](#)
26. Diogo MC, Glatter S, Prayer D, et al. **Improved neurodevelopmental prognostication in isolated corpus callosal agenesis: fetal magnetic resonance imaging-based scoring system.** *Ultrasound Obstet Gynecol* 2021;58:34–41 [CrossRef Medline](#)
27. Atallah A, Lacalm A, Massoud M, et al. **Prenatal diagnosis of pericallosal curvilinear lipoma: specific imaging pattern and diagnostic pitfalls.** *Ultrasound Obstet Gynecol* 2018;51:269–73 [CrossRef Medline](#)
28. Shinar S, Lerman-Sagie T, Telleria ME, et al. **Fetal pericallosal lipomas: clues to diagnosis in the second trimester.** *Eur J Paediatr Neurol* 2018;22:929–34 [CrossRef Medline](#)
29. Chougar L, Blondiaux E, Moutard ML, et al. **Variability of T1-weighted signal intensity of pericallosal lipomas in the fetus.** *Pediatr Radiol* 2018;48:383–91 [CrossRef Medline](#)
30. Glatter S, Kasprian G, Bettelheim D, et al. **Beyond isolated and associated: a novel fetal MR imaging-based scoring system helps in the prenatal prognostication of callosal agenesis.** *AJNR Am J Neuroradiol* 2021;42:782–86 [CrossRef Medline](#)